ACS OMEGA

http://pubs.acs.org/journal/acsodf

Article

Probing the Effect of Halogen Substituents (Br, Cl, and F) on the Non-covalent Interactions in 1-(Adamantan-1-yl)-3-arylthiourea Derivatives: A Theoretical Study

Lamya H. Al-Wahaibi, Divya Sri Grandhi, Samar S. Tawfik, Nora H. Al-Shaalan, Mohammed A. Elmorsy, Ali A. El-Emam, M. Judith Percino, and Subbiah Thamotharan*

Cite This: *ACS Omega* 2021, 6, 4816−4830

Read Online

ACCESS | Metrics & More | Article Recommendations | Supporting Information

ABSTRACT: The effect of halogen substituents (X = Br, Cl, and F) on the crystal packing and intra- and intermolecular interactions in four adamantane−thiourea hybrid derivatives is investigated using different theoretical tools. The bromo and chloro derivatives exhibit 3D isostructurality as evident from lattice parameters, molecular conformation, and crystal packing. The density functional theory study suggests that the molecular conformation of the parent (unsubstituted) and fluoro derivatives exhibits a stable low energy anti−syn conformation. In contrast, bromo and chloro derivatives adopt stable and relatively high energy minima on their potential energy surfaces. Hirshfeld surface analysis reveals the effect of halogen substituents on the intermolecular contacts. The halogen atoms mainly reduce the contribution of H···H contacts toward crystal packing. PIXEL energy analysis indicates the strong dimer formed by N−H···S hydrogen bonds in all four structures. It also revealed that a vast number of H···H contacts observed in different dimers of these structures either presented along with other conventional interactions or solely stabilize the dimeric topology. The topological parameters for intermolecular interactions in these structures suggest an intermediate bonding character between shared and closed-shell interactions for N−H···S hydrogen bonds in the parent and chloro derivatives. In contrast, the N−H···S hydrogen bond in other structures is of a closed-shell interaction. Among four derivatives, the fluoro derivative is weakly packed in the solid state based on the PIXEL method's lattice energy calculation.

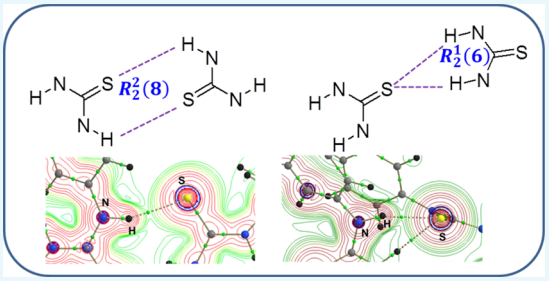

INTRODUCTION

Adamantane-based derivatives were recognized early as potent chemotherapeutic agents possessing antiviral,[1−5] anticancer,[6−10] antituberculosis,[11,12] antifungal,[13] and antiprotozoal[14−17] activities. On the other hand, thiourea derivatives were proved to possess diverse chemotherapeutic properties including anticancer,[18−20] antiviral,[21−23] antituberculosis,[24] and antimalarial activities.[25] In addition to diverse biological activities, thiourea derivatives are utilized as precursors for biologically active derivatives.[26−28] In view of the above, we prepared 1-(adamantan-1-yl)-3-arylthiourea derivatives, and brief structural reports were described earlier.[29−33] The reported structures revealed that the thiourea moiety adopted two different conformations such as anti−anti and anti−syn conformations. The bromo and chloro derivatives adopted the anti−anti conformation, whereas the unsubstituted derivative and the *p*-fluoro derivative exhibited the anti−syn conformation. The antitubercular drug isoxyl (*N*,*N*′-[4-(3-methylbutoxy)phenyl]thiourea] crystallized in two conformational polymorphic forms (csd refcode: QQQDVM02 and QQQDVM03) in which the thiourea moiety adopted anti−anti and anti−syn conformations.[34] Another drug molecule (drug bank ID: DB07004),[35] namely, 2-[(5-hex-1-yn-1-ylfuran-2-yl)carbonyl]-*N*-methylhydrazinecarbothioamide, was found to be known that the thiourea moiety adopts the anti−syn conformation when it complexes with a metal binding protein, S100-B.[36] A similar anti−syn conformation was observed in a small inhibitor, (*N*-[[3-fluoro-4-ethoxy-pyrid-2-yl]ethyl]-*N*′-[5-nitrilomethyl-pyridyl]-thiourea), which contains the thiourea unit drug molecule when bound at the active site of the HIV-1 reverse transcriptase.[37] The amino group in the syn orientation is involved in the hydrogen bonding interaction with the active-site residue of the HIV-1 reverse transcriptase.

Therefore, it is crucial to investigate the conformational preference of molecules with medicinal values. The previous structural studies of the title 1-(adamantan-1-yl)-3-arylthiourea derivatives did not provide details on the halogen substituent effect and conformational importance of anti−anti and anti−

Received: November 28, 2020
Accepted: February 2, 2021
Published: February 10, 2021

Scheme 1. Synthesis of Compounds 1−4 from Adamantan-1-yl Isothiocyanate A and Primary Aromatic Amines B

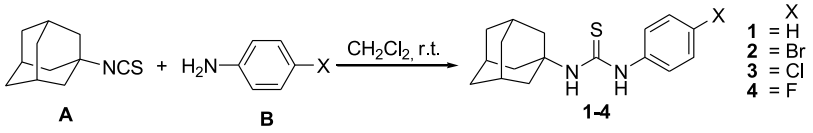

syn conformations of the thiourea unit present in them. To obtain a better understanding of the molecular conformation, the role of non-covalent interactions to the crystal packing, and the effect of different halogen substituents, we have performed different theoretical analyses using the reported 3D structures of 1-(adamantan-1-yl)-3-arylthiourea derivatives.[30−33] Moreover, a complete understating of weak non-covalent forces is vital to generate a new application in different disciplines. The molecular properties of crystalline solids primarily depend on the molecular arrangement, and various non-covalent forces control this arrangement. Different types of hydrogen bonding interactions including N/O−H···O/N/S interactions and other types of weak non-covalent interactions such as C−H···O/N/S/X/π (where X is halogen), $\pi\cdots\pi$ stacking, halogen bonds, chalcogen bonds, and so forth play essential roles in governing the self-assembly of a given molecule.

In this work, we report the modified synthesis procedure for four 1-(adamantan-1-yl)-3-arylthiourea derivatives, and three of them contain halogens (Br, Cl, and F) in the para position of the aryl ring (Scheme 1) with a better yield in comparison with previously reported procedures. Besides, the effect of different halogen substituents is qualitatively analyzed using the Hirshfeld surface (HS) tool. Further, we employed Gavezzotti's PIXEL method for studying the strength of different dimeric topologies formed in these structures. The most strong dimer was formed by the N−H···S hydrogen bond in all four structures. In the unsubstituted and fluoro derivatives of the title compounds, the N−H···S hydrogen bond generates a $R_2^2(8)$ ring motif when thiourea adopts an anti−syn conformation. Eccles et al. investigated the N−H···S═C synthon in a series of primary aromatic thioamides and co-crystals of the halogen bond donor moiety 1,4-diiodotetrafluorobenzene with aromatic thioamides.[38,39] The amino group in the syn orientation generates a $R_2^2(8)$ ring motif, while the amino group in the anti orientation produces a C(4) chain, and these two motifs combined to lead to a supramolecular ladder motif.[38] In the above co-crystal complexes, either the C(4) chain or $R_2^2(8)$ ring had formed.[39] The adamantane−thiourea hybrid derivatives reported earlier showed anti−anti and anti−syn conformations for the thiourea moiety. In these structures, the NH group in the anti orientation has involved in an intramolecular N−H···O═C hydrogen bond, which locks the overall conformation of the molecule, and the NH group in the syn orientation has participated in an intermolecular N−H···S═C hydrogen bond.[40−43] Similarly, some substituted benzoylthiourea[44] and thiocarbamide[45] derivatives also showed anti−anti and anti−syn conformations for the thiourea moiety with an intramolecular N−H···O═C hydrogen bond.

A CSD search (CSD version 5.41, March 2020 update)[46] was conducted [conditions used: (i) 3D coordinates determined, (ii) only non-disordered, (iii) no errors, (iv) not polymeric, (v) no ions, (vi) only single-crystal structures, and (vii) only organics] to see the frequency of this motif. The results suggested that there are 1722 hits possessing this motif. The $R_2^1(6)$ motif observed in the bromo and chloro derivatives of the title compounds which prefer to form an anti−anti conformation and the CSD search for this motif yielded 111 hits. The fragments used for the CSD search are depicted in Figure 1. Furthermore, Bader's quantum theory of the atoms-

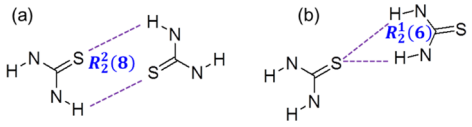

Figure 1. Fragments used for the CSD search: anti−syn (a) and anti−anti (b) conformers of thiourea.

in-molecules approach (QTAIM)[47,48] was used to characterize the non-covalent interactions found in these structures. The adamantane-containing structures display characteristic short H···H contacts (H−H bonding), and these contacts orchestrated in a non-electrostatic manner. The topological parameters are used to delineate the strength of these close contacts along with the conventional non-covalent interactions in the present work.

RESULTS AND DISCUSSION

In the present investigation, we describe the conformational preference of molecules of four adamantane−arylthiourea hybrid derivatives with para-substituents (H, Br, Cl, and F) on the phenyl ring and explored the roles of weak non-covalent interactions present in them using various theoretical approaches including HS analysis, PIXEL energy analysis, and topological analysis of the electron density for non-covalent interactions.

Molecular Conformation. The molecular structures of compounds **1−4** are represented in the ball-and-stick model, as shown in Figure 2. From this figure, we can see that the thiourea moiety adopts two different conformations, that is, anti−anti and anti−syn conformations concerning the amine H and S atoms of the thiourea moiety (rotation about the C−N bond). The anti−anti conformation is observed in the parent and the fluoro derivatives, while the anti−syn conformation is preferred by the bromo and chloro derivatives. The same anti−syn conformation was also observed in a related structure in which chlorine is attached at the meta position of the phenyl ring (CSD refcode: **RAPNOO**).[29]

In order to obtain the conformational landscape of title molecules, we carried out a relaxed potential energy surface (PES) scan around C−N bonds (dihedral angles T1 and T2) of the thiourea unit. Figure 3 shows the energy change as a function of the C−N bond rotation. For molecule 1, dihedral angles T1 = −170° (anti; X-ray: −170.2°) and T2 = −10° (syn; X-ray: 7.4°) produced the least energy conformers. The second least energy conformer was obtained for T1 = −5°. The energy difference between anti and syn orientations for T1 is ca. 6.5 kcal mol^{-1}. In the case of T2, the syn orientation is 5 kcal mol^{-1} more stable than the anti conformation. For molecule 4, the minimum energy conformers have dihedral angles T1 = ±170° (anti; X-ray: 176.6°) and T2 = −10° (syn; X-ray: −1.5°). There is a similar energy difference between the

https://dx.doi.org/10.1021/acsomega.0c05793
ACS Omega 2021, 6, 4816−4830

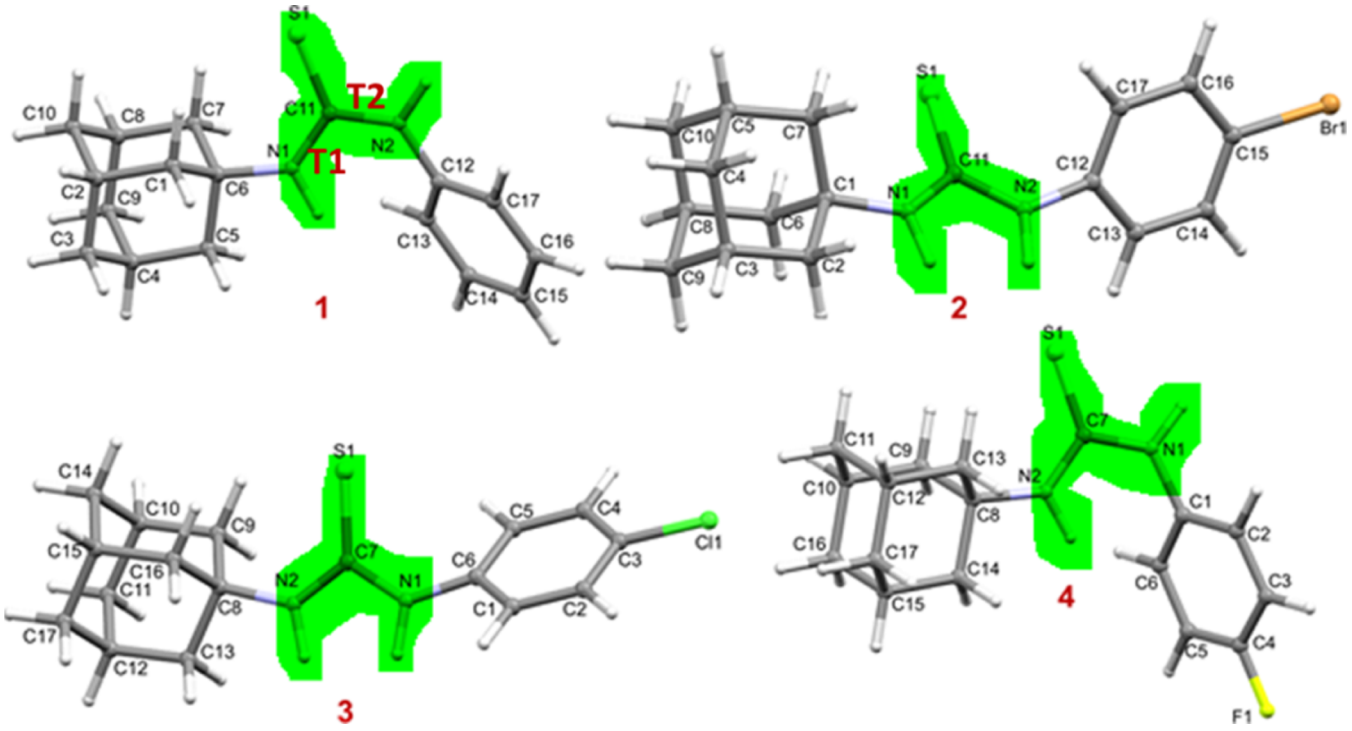

Figure 2. Ball and stick representation of molecules of **1**−**4** and with the atom-labeling scheme as in the crystallographic information file. The representative dihedral angles (T1: H-N1-C11-S1 and T2: H-N2-C11-S1) are indicated.

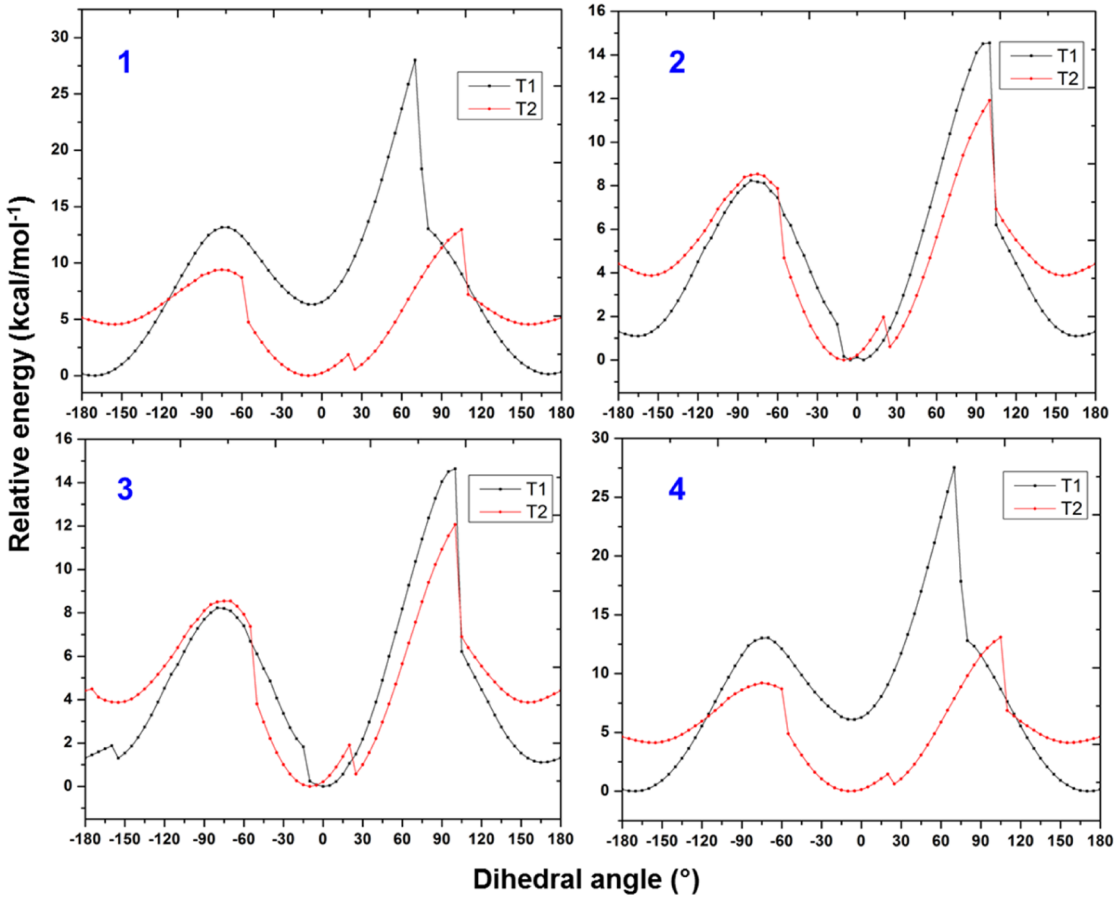

Figure 3. Calculated potential energy for rotation around the C−N bonds (T1 and T2 as shown in Figure 2) in structures **1**−**4**.

https://dx.doi.org/10.1021/acsomega.0c05793
ACS Omega 2021, 6, 4816−4830

anti and syn conformations for the T1 (6.1 kcal mol^{-1}) and T2 (4.6 kcal mol^{-1}) dihedral angles as observed in 1.

In 2, the energy difference between syn and anti conformations for the T1 dihedral angle is 1.0 kcal mol^{-1} (minimum energy conformer at T1 = 5°; X-ray: 172.8°), and the corresponding value is 4.2 kcal mol^{-1} for the T2 dihedral angle (minimum energy conformer at T2 = −10°; X-ray: −168.6°). A similar rotational barrier trend is noticed for molecule 4 (T1 = 0°; X-ray: −172.8° and T2 = −10°; X-ray: 167.2°).

This analysis indicates that molecules **1** and **4** showed similar rotational barriers, while molecules with Cl (**2**) and Br (**3**) substituents displayed similar energy profiles. The minimum energy conformers identified from the PES scan analysis agree with X-ray conformations of **1** and **4**, whereas molecules **2** and **3** crystallized with relatively high energy minima (anti−anti conformation) as compared to low energy minima (anti−syn conformation). Furthermore, the modeled structures with anti−anti and anti−syn conformations were subjected to structural optimization to identify the most stable conformer at the M06-2X/cc-pVTZ level of theory. The results suggest that the anti−syn conformer is the most stable over the anti−anti conformer by 3.4−4.1 kcal mol^{-1} in all four structures. The torsion angles describe the anti−anti and anti−syn conformations, which are listed in Table S1. Saeed et al. explored the rotational barriers for anti−syn (S conformation) and anti−anti (U conformation) in some of the thiourea-containing derivatives.[49,50] The authors have reported that the S conformation was more stable by 11.8−13 kcal mol^{-1} than the U conformation, and these values are relatively higher than those in the present work. This feature suggests that the transition between anti−syn and anti−anti conformers is much easier in the title derivatives.

Further, the adamantane moiety contains four fused six-membered rings, and these rings adopt a chair conformation as observed in related adamantane structures.[51−53] The chair conformation is confirmed by the Cremer and Pople puckering parameters.[54]

Intramolecular Interactions in Anti−Syn and Anti−Anti Conformers. We performed a topological analysis for the crystal structure geometry (with normalized H positions) to understand how these low- and high-energy conformers stabilized. As shown in Figure 4, the molecular conformation was stabilized by two intramolecular C−H···S interactions in all four structures. In the most stable anti−syn conformers, there is an additional N−H···C(π) interaction that is observed. The N−H group in the anti conformation has participated in the N−H···C(π) interaction and stabilizes the anti−syn conformer. The topological parameters for intramolecular interactions are summarized in Table S2. The dissociation energies for C−H···S and N−H···C(π) interactions are comparable, and the strength of the N−H···C(π) interaction is relatively stronger than the C−H···S interaction.

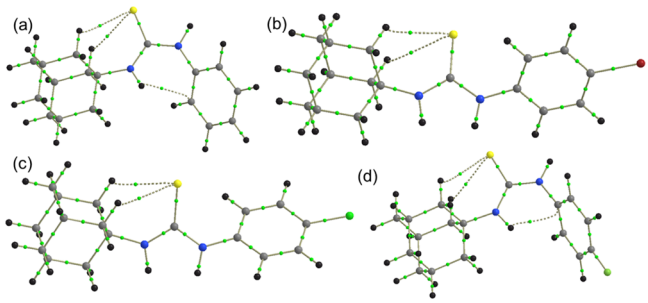

Figure 4. Molecular graphs showing intramolecular interactions in the structures of **1** (a), **2** (b), **3** (c), and **4** (d).

Hirshfeld Surface Analysis. The HS analysis was performed to qualitatively measure differences and similarities of the various intermolecular interactions. This analysis also helps to understand how these intercontacts varied due to halogen substituents. The results suggest the H···H contacts to be the most significant interactions in all four structures ranging from 74.1 to 56.1%. As expected, the maximum contribution comes from H···H contacts in the parent compound. All three halogen substituents reduce the contribution of H···H contacts ranging from 13.1 to 18%, and H···X contacts compensate for this reduction. It should be noted that halogens do not alter the contribution of H···S and H···C contacts. These contacts contribute around 10−11% in all four structures. Similar features are also noted when the chlorine substituent is attached at the meta position of the phenyl ring (3-Cl, csd refcode: **RAPNOO**).[29] We can see from Figure 5 the large and intense red areas shown for the N−H···S interaction, suggesting its vital role in the stabilization.

2D fingerprint plots for various key intercontacts show some similar and dissimilar features of contact distances. The shortest H···H contacts are located around 2.1 Å in **1**, 2.2 Å in **2** and **3**, and 2.4 Å in **4** (Figure 6). Since bromo (**2**) and chloro (**3**) derivatives are isotypic, the decomposed 2D fingerprint plots for different intercontacts are very similar. The closest H···S contacts appear at 2.4 Å in **1**−**3**, with the corresponding distance located at 2.5 Å in **4**. Further, the H···C contacts appear at a longer distance (∼2.9 Å) in **4** compared to other structures. The distribution of H···F contacts is different from H···Br/Cl contacts.

Analysis of Molecular Electrostatic Potentials. As shown in Figure 7, the molecular electrostatic potential (MESP) map reveals invariant and variable features for these structures. In all four structures, the MESP shows the presence of the σ-hole at the S atom with the positive electrostatic potential ($V_{s,max}$) value ranging from −16.5 to −19.3 kcal mol^{-1} and a characteristic negative ($V_{s,min}$) belt around the S atom. The positive and negative electrostatic potentials are comparable between parent and fluoro derivatives and between bromo and chloro derivatives. Similarly, the σ-holes are also seen at halogen atoms in structures **2**−**4**. The $V_{s,max}$ values along the C−X bond is positive in the bromo (9.3 kcal mol^{-1}) and chloro (2.9 kcal mol^{-1}) derivatives, whereas the corresponding value is negative (−10.0 kcal mol^{-1}) in the fluoro derivative. The negative belt around halogen atoms corresponds to the lone pair electrons, and the $V_{s,min}$ values are comparable in halogen derivatives. In parent and fluoro derivatives, the N−H proton's donating tendency in the syn conformation is more than the N−H proton in an anti conformation (26.2 kcal mol^{-1} in **1** and 24.2 kcal mol^{-1} in **4**) based on the $V_{s,max}$ values. We note that a single positive electrostatic potential is located between amino protons in **2** and **3**. This feature suggests that the donating strength of the amino protons has increased in the anti−anti conformation.

Molecular Dimers and Crystal Packing of 1−4. The molecular dimers were extracted from the crystal structures of **1**−**4** based on the intermolecular interaction energies calculated by the PIXEL method (Table 1). These dimers are ranked according to the net intermolecular interaction

https://dx.doi.org/10.1021/acsomega.0c05793
ACS Omega 2021, 6, 4816−4830

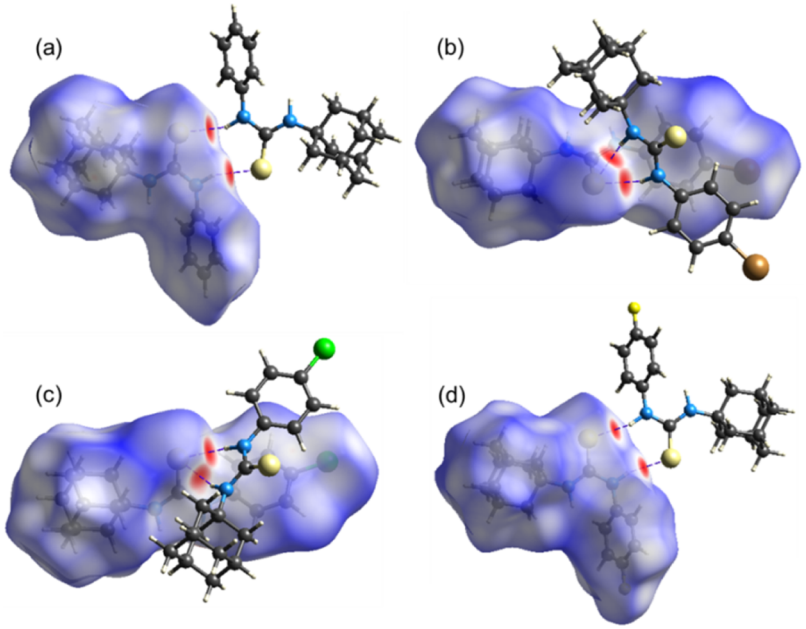

Figure 5. HS highlighting the short N−H···S hydrogen bonds in structures of **1** (a), **2** (b), **3** (c), and **4** (d).

energies. The crystal packing and dimers observed in molecules **1**−**4** are discussed in a separate section.

Molecular Dimers of 1. Molecules of compound **1** are packed as layers of helical chains, and these layers run parallel to the crystallographic *c*-axis as depicted in Figure 8. The PIXEL energy analysis reveals six molecular dimers (I−VI; Figure 8b−g) found to be energetically significant, and the total intermolecular interaction energies for these dimers range from −17.3 to −1.6 kcal mol^{-1}. The molecular dimers found in this structure are illustrated in Figure 8. The strong dimer in this structure stabilizes by an intermolecular N−H···S interaction, and the electrostatic energy contributes about 76% toward the stabilization of this dimer. A $R_2^2(8)$ synthon is formed by this N−H···S interaction. Other dimers are found to be relatively weaker than dimer I, and four of these dimers (II−V) are primarily stabilized by intermolecular C−H···S and C−H···C(π) interactions. We note that one of the amino groups (N1−H) of the thiourea moiety is not involved in intermolecular interactions.

Further, an extensive number of short H···H contacts (2.13 to 2.34 Å) provide additional stability to the respective dimers. It is important to note that the H···H contacts are of the type Csp^3−H···H−Csp^2 and Csp^3−H···H−Csp^3 interactions. Short H···H contacts are one of the characteristic features observed in the adamantane-containing crystal structures and play a key role in stabilizing the crystal structure in a non-electrostatic nature.[55−57]

Furthermore, the adjacent adamantane cores interact *via* Csp^3−H···H−Csp^3, and the adamantane core interlinks with the phenyl ring *via* the Csp^3−H···H−Csp^2 interaction. Except in dimer I, the dispersion energy component plays an essential role in the stabilization of these dimers. The dispersion energy ranges from 67 (dimer III) to 75% (dimer IV) toward the stabilization of these dimers. Molecules of **1** form as a helical chain in the solid state, and this spiral-like chain is formed by dimers II, III, V, and VI. This feature suggests that short H···H contacts help link the molecules of **1** in the solid state.

Molecular Dimers in the Bromo Derivative (2) and Its Chloro Counterpart (3). The crystal structures of the bromo (**2**) and chloro (**3**) derivatives are isostructural, as evident from the cell parameters and the space group [**2**: a = 17.0675 (7), b = 8.3422 (3), c = 22.5970 (8) Å, *Pbca* and **3**: a = 17.2134 (6), b = 8.2251 (2), c = 22.5220 (7) Å, *Pbca*]. The number of energetically significant dimers observed in the bromo and chloro derivatives is slightly different. In the former structure, there are eight dimers, and these dimers are held together by various intermolecular interactions such as N−H···S, N−H···C(π), C−H···S, and C−H···Br interactions and H···H short contacts. The intermolecular N−H···S, N−H···C(π), C−H···S, and C−H···Cl interactions and H···H short contacts in addition to C···C and C···Cl contacts observed in the seven dimers of the latter structure. The crystal packing of **2** and its dimers observed in the solid state are illustrated in Figures 9 and 10.

The molecules of the bromo and chloro derivatives form as 2D-columnar packing along the crystallographic *ac*-plane. As highlighted in Figure 9a, the basic motif observed in these structures is formed by three centered N−H···S interactions (dimer I in **2** and **3**; Figure 9b). The molecular layers run parallel to the *c*-axis, and the adjacent layers run in an anti-parallel fashion.

Both the amino groups of the thiourea moiety act as donors, and the S atom of the thiourea unit involves as an acceptor. Further, intermolecular N−H···C(π) interactions provide additional stability to this dimer in **2**. In **3**, the presence of secondary interactions such as C···C and C···Cl-type contacts is observed in dimer I along with three centered N−H···S and one N−H···C(π) interaction. These secondary interactions could increase this dimer's stability in **3**, as evident from the intermolecular interaction energies compared to the structure of **2**.

The stability of other dimers is weaker than that of dimer I in both **2** and **3**, and the strength of these dimers is also comparable in these isotypic structures. The second most stable dimer (II, E_{tot}: −3.8 kcal mol^{-1}) is formed by a C−H···S interaction, and a short Csp^2−H···H−Csp^3 contact provides additional stability to this dimer. These interactions link the molecules into a chain that runs parallel to the *b*-axis. Further,

https://dx.doi.org/10.1021/acsomega.0c05793
ACS Omega 2021, 6, 4816−4830

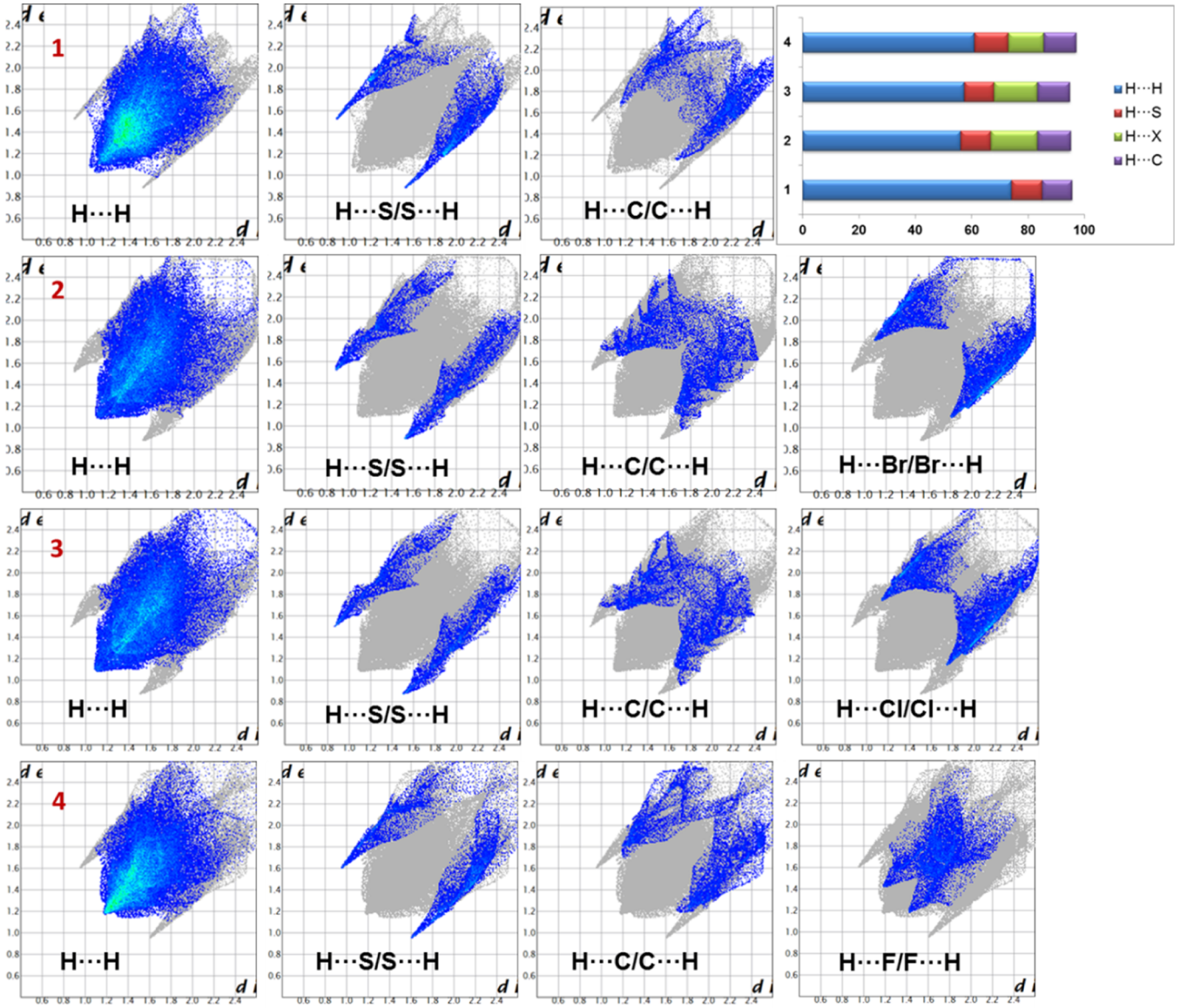

Figure 6. 2D fingerprint plots for key intermolecular contacts observed in structures **1**–**4**. Top right panel: the relative contributions of these contacts.

the dispersion energy contributes about 65% toward the stabilization of dimer II. In **2** and **3**, three dimers form purely by short H···H contacts of the types Csp^2–H···H–Csp^3 and Csp^3–H···H–Csp^3 interactions. As mentioned above, the number of C–H···Br/Cl interactions is different. The dimers formed by C–H···Br interactions (VI–VIII; Figure 10a–c) are weaker than dimers stabilized by short H···H contacts in **2**, whereas one of the dimers formed by the C–H···Cl (IV) interaction is slightly stronger than H···H-mediated dimers in **3**.

One of the C–H···Br interactions (dimer VIII) is found to be a short interaction compared to the other two C–H···Br interactions. In all three C–H···Br-mediated dimers, the adamantyl core functions as a donor, and these interactions individually link the molecules into a chain. The dimers formed in **3** are depicted in Figure 11a–g, and the crystal packing of **3** is illustrated in Figure S1 (Supporting Information). In **3**, one of the C–H···Cl interactions (dimer VII) is a short interaction compared to another C–H···Cl interaction (dimer IV). As observed in **2**, these two interactions interconnect the molecules into a chain.

Molecular Dimers in the Fluoro Derivative (4). Molecules of compound **4** are arranged as linear chains that run parallel to the *b*-axis and the layer arrangement in the crystallographic *bc*-plane, as shown in Figure 12a. It possesses entirely different crystal packing compared to the parent and Br/Cl derivatives. The PIXEL energy analysis indicates seven molecular dimers (I–VII) which are found to be energetically significant, and the total intermolecular interaction energies for these dimers range from −16.3 to −1.9 kcal mol^{-1}. The molecular dimers observed in **4** are illustrated in Figure 12b–h. The most strong dimer (I) forms by intermolecular N–H···S and C–H···S interactions, and this dimer is predominantly electrostatic in nature with the contribution of 75%. Further, the stability of this dimer is relatively less compared to that of other strong dimers formed by the N–H···S interaction due to the slightly longer separation of H and S with the value of 2.56 Å.

https://dx.doi.org/10.1021/acsomega.0c05793
ACS Omega 2021, 6, 4816–4830

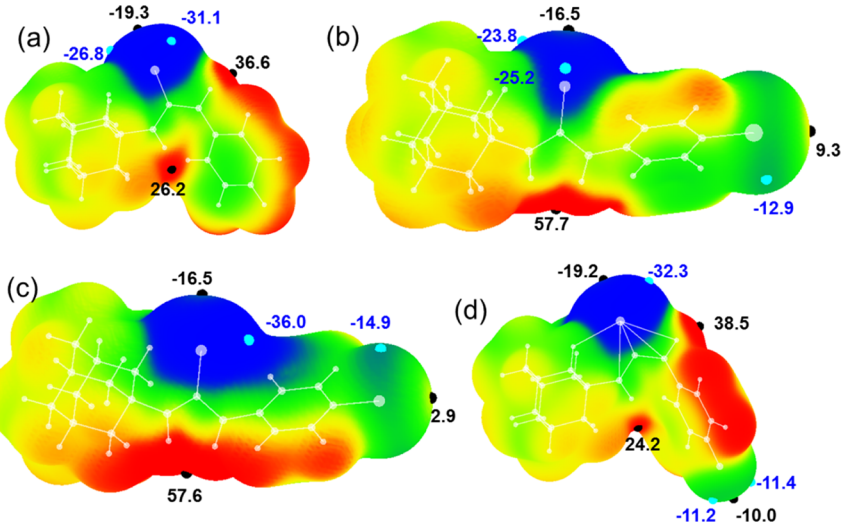

Figure 7. MESP surface plots of **1** (a), **2** (b), **3** (c), and **4** (d). Color scales (in kcal mol^{-1}): red: more than 15; yellow: 0−15; green: −15 to 0; blue: above −15.

The next potent dimer (II) stabilizes by the intermolecular C−H···S interaction, and the energy for this dimer is comparable to that of dimer II in **1**. However, the dimer's stability is stronger than the dimers mediated by the C−H···S interaction in Br/Cl derivatives. In this structure, three dimers (III, IV, and VI) stabilize by H···H contacts, and the former dimers are established slightly longer than the sum of the van der Waals (vdW) radii of H atoms as observed in different organic molecular structures.[58] In the latter dimers, the H···H intercontacts are within the sum of the vdW radii of H atoms. However, the stability of these H···H-mediated dimers is relatively stronger than those of dimers formed by H···H contacts in other structures. In the H···H-mediated dimers, the adjacent adamantyl cores are interconnected by the Csp^3−H···H−Csp^3 type of interaction.

Among two intermolecular C−H···F interactions (V and VII), one of the C−H···F interactions (V) generates a closed molecular loop. Although this interaction is established with the sum of the vdW radii of H and F + 0.19 Å, the intermolecular interaction energy for this dimer is found to be stronger than those for dimers formed by C−H···Br/Cl interactions. As the molecular chain was formed by C−H···Br/Cl interactions in **2** and **3**, the second C−H···F interaction also interlinks the molecules of **4** into a chain that runs parallel to the crystallographic *b*-axis.

Analysis of Lattice Energies. The lattice energies for compounds **1**−**4** and one of the closely related structures of urea derivatives containing the Br substituent (csd refcode: **RAPNII**) were calculated using the PIXEL method. The net lattice energy and its components are summarized in Table 2. The result indicates that the bromo and chloro derivatives with the thiourea unit show comparable lattice energies as expected due to isotypic nature. Moreover, these crystals display more stability than the parent and fluoro derivatives. The electrostatic and dispersion energy components contribute about 46−47 and 54−53% to the bromo and chloro derivatives, respectively. A similar percentage of dispersion energy contributed to the stabilization of thione derivatives.[40]

The parent compound is slightly more stable compared to the fluoro derivative (**4**). The different energy components of net lattice energy suggest that the parent crystal's repulsion and dispersion energy are significantly higher. These features indicate that the fluorine substituent plays a vital role in reducing the stability of the crystal. The contribution of the dispersion energy is 62% toward the stabilization of the fluoro derivatives. The corresponding value is decreased slightly, about 60% to the parent compound's stabilization. It is interesting to note that when the urea moiety replaces thiourea in **2**, then the resulting crystal (**RAPNII**) reduces the stability by 7 kcal mol^{-1}. However, the contributions of dispersion (55%) and electrostatic (45%) energies are nearly the same in urea (**RAPNII**) and thiourea (**2**) containing Br derivatives. When the para Cl substituent is moved to the meta position (**RAPNOO**), the stability of the 3-Cl crystal is reduced by 3.7 kcal mol^{-1}. The electrostatic contribution is also reduced by 6% toward the stabilization of **RAPNOO** compared to its para isomer (**3**).

Topological Features of Intermolecular Interactions. The topological parameters were calculated for all intermolecular interactions summarized in various dimers of compounds **1**−**4** (Table 1) within the framework of QTAIM in order to quantify the strength of the individual intermolecular interaction. The molecular graphs for all dimers of **1**−**4** are illustrated in Figures S2−S5 (Supporting Information). In all four structures, the strong dimer is primarily stabilized by either a single N−H···S interaction (in **1** and **4**) or three centered N−H···S interactions (in **2** and **3**). The KP-4 rule differentiates vdW interactions from hydrogen bonds, and different types of hydrogen bonds observed in **1**−**4** structures are summarized in Table 3 along with their topological properties. The topological parameters for other non-covalent interactions are presented in Tables S3−S6 (Supporting Information). The electron density values for hydrogen bonds lie within the Koch and Popelier proposed limit in the range of 0.013−0.236 e $Å^{-3}$ for typical hydrogen bonds.[59] The Laplacian of the electron density values for N−H···S hydrogen bonds is found within the suggested limit of 0.580−3.355 e $Å^{-5}$, and other hydrogen bonds are not within this limit.

Further, the $\nabla^2\rho(r) > 0$, $|-V(r)/G(r)| > 0$, and $H(r) < 0$ conditions indicate that the N2−H21···S1 hydrogen bond in **1** and the N1−H20···S1 hydrogen bond in **3** show increasing

https://dx.doi.org/10.1021/acsomega.0c05793
ACS Omega 2021, 6, 4816−4830

Table 1. Intermolecular Interaction Energies (in kcal mol^{-1}) for Various Dimers Obtained by the PIXEL Method in the Crystal Structures of 1−4[a]

motif	CD	symmetry	important interactions	geometry H···A (Å), ∠D−H···A (deg)	E_{Coul}	E_{pol}	E_{disp}	E_{rep}	E_{tot}	ΔE_{cp}
				Compound **1**						
I	8.285	$-x, -y + 2, -z + 1$	N2−H21···S1	2.43, 157	−16.9	−10.8	−8.7	19.0	−17.3	−14.0
II	5.641	$-x + 1/2, y + 1/2, z$	C5−H8···S1	3.10, 141	−3.7	−2.4	−13.0	9.5	−9.5	−10.4
			H2···H11	2.34						
			H2···H14	2.13						
			C11−S1···*Cg*1	3.993 (7), 76.89(4)						
III	8.451	$x - 1/2, -y + 3/2, -z + 1$	C15−H18···S1	3.09, 134	−2.2	−1.6	−7.6	5.4	−6.0	−5.1
			H7···H19	2.29						
IV	6.764	$-x + 1, -y + 2, -z + 1$	C9−H12···C14	2.85, 143	−1.4	−0.9	−6.8	4.2	−4.9	−4.2
			H9···H17	2.31						
V	9.053	$x + 1/2, y, -z + 1/2$	C3−H5···S1	3.08, 174	−1.7	−1.1	−6.0	5.0	−3.9	−4.7
			H13···H1	2.24						
VI	11.741	$x, -y + 3/2, z - 1/2$	H5···H18	2.28	−0.8	−0.5	−3.1	2.7	−1.6	−1.5
				Compound **2**						
I	4.423	$-x + 3/2, y - 0.5, z$	N1−H20···S1	2.43, 159	−16.7	−11.3	−20.4	27.8	−20.6	−19.0
			N1−H20···C12(π)	2.84, 120						
			N2−H21···S1	2.43, 159						
			N2−H21···C17(π)	2.81, 118						
II	8.363	$-x + 1, y - 0.5, -z + 0.5$	C5−H6···S1	2.94, 123	−2.0	−1.7	−6.8	6.7	−3.8	−4.5
			H6···H19	2.22						
III	15.177	$-x + 1, -y + 1, -z$	H14···H14	2.28	−1.5	−0.7	−5.2	4.6	−2.8	−2.8
			H14···H11	2.39						
IV	11.311	$x, -y + 3/2, z - 0.5$	H11···H18	2.24	−1.0	−0.4	−3.2	1.7	−2.8	−2.1
V	8.688	$x + 0.5, y, -z + 0.5$	H15···H17	2.39	−0.4	−0.6	−4.1	2.4	−2.7	−2.3
VI	11.963	$-x + 3/2, -y + 1, z - 0.5$	C3−H3···Br1	3.08, 132	−1.1	−0.3	−3.1	2.1	−2.4	−2.5
VII	12.045	$x - 0.5, y - 1, -z + 0.5$	C4−H4···Br1	3.15, 174	−0.4	−0.2	−2.6	1.2	−2.0	−1.7
VIII	12.323	$-x + 3/2, -y + 2, z - 0.5$	C8−H11···Br1	2.93, 134	−0.7	−0.3	−2.5	1.8	−1.7	−1.2
				Compound **3**						
I	4.671	$-x + 3/2, y - 1/2, z$	N1−H20···S1	2.39, 162	−17.2	−12.0	−20.5	28.5	−21.2	−19.1
			N1−H20···C5(π)	2.81, 115						
			N2−H21···S1	2.45, 158						
			C5···C3	3.378(1)						
			C5···Cl1	3.573(1)						
II	7.606	$-x + 1, y - 1/2, -z + 3/2$	C10−H7···S1	2.91, 125	−1.9	−1.8	−6.7	6.6	−3.8	−4.4
			H7···H4	2.21						
III	11.341	$x, -y + 3/2, z - 1/2$	H15···H3	2.22	−1.0	−0.4	−3.3	1.9	−2.8	−2.1
IV	11.805	$-x + 3/2, -y + 1, z - 1/2$	C12−H10···Cl1	3.03, 132	−0.9	−0.3	−3.3	1.8	−2.7	−2.4
V	8.612	$x - 1/2, y, -z + 3/2$	H2···H14	2.37	−0.4	−0.6	−4.0	2.3	−2.7	−2.1
VI	13.490	$-x + 1, -y + 1, -z + 2$	H13···H13	2.25	−1.6	−0.7	−5.1	4.9	−2.4	−2.8
VII	12.709	$-x + 3/2, -y + 2, z - 1/2$	C15−H15···Cl1	2.91, 136	−0.4	−0.3	−2.2	1.1	−1.7	−1.1
				Compound **4**						
I	8.228	$-x, -y + 2, -z + 1$	N1−H20···S1	2.56, 140	−15.1	−8.3	−8.0	15.0	−16.3	−13.4
			C2−H1···S1	3.05, 123						
II	7.011	$-x + 1, -y + 2, -z + 1$	C3−H2···S1	2.89, 142	−5.2	−2.8	−10.2	7.3	−10.9	−9.6
III	6.492	$-x, -y + 1, -z$	H4···H7	2.46	−1.8	−1.2	−8, 8	4.4	−7.4	−6.7
			H4···H17	2.46						
IV	6.427	$x - 1, y, z$	H6···H14	2.37	−1.7	−1.6	−8.6	5.0	−6.9	−7.3
			H7···H15	2.39						
			H9···H18	2.38						
V	6.949	$-x + 1, -y + 1, -z$	C16−H16···F1	2.86, 145	−0.8	−0.8	−7.3	3.9	−5.0	−4.8
VI	9.369	$-x, -y + 1, -z + 1$	H9···H11	2.36	−1.0	−0.7	−4.7	2.3	−4.1	−4.3
VII	12.669	$x - 1, y - 1, z$	C11−H8···F1	2.61, 134	−0.6	−0.2	−2.2	1.2	−1.9	−1.7

[a]Neutron values are given for all D−H···A interactions. CD: centroid-to-centroid distance of the molecular pair. *Cg*1: centroid of the phenyl ring.

https://dx.doi.org/10.1021/acsomega.0c05793
ACS Omega 2021, 6, 4816−4830

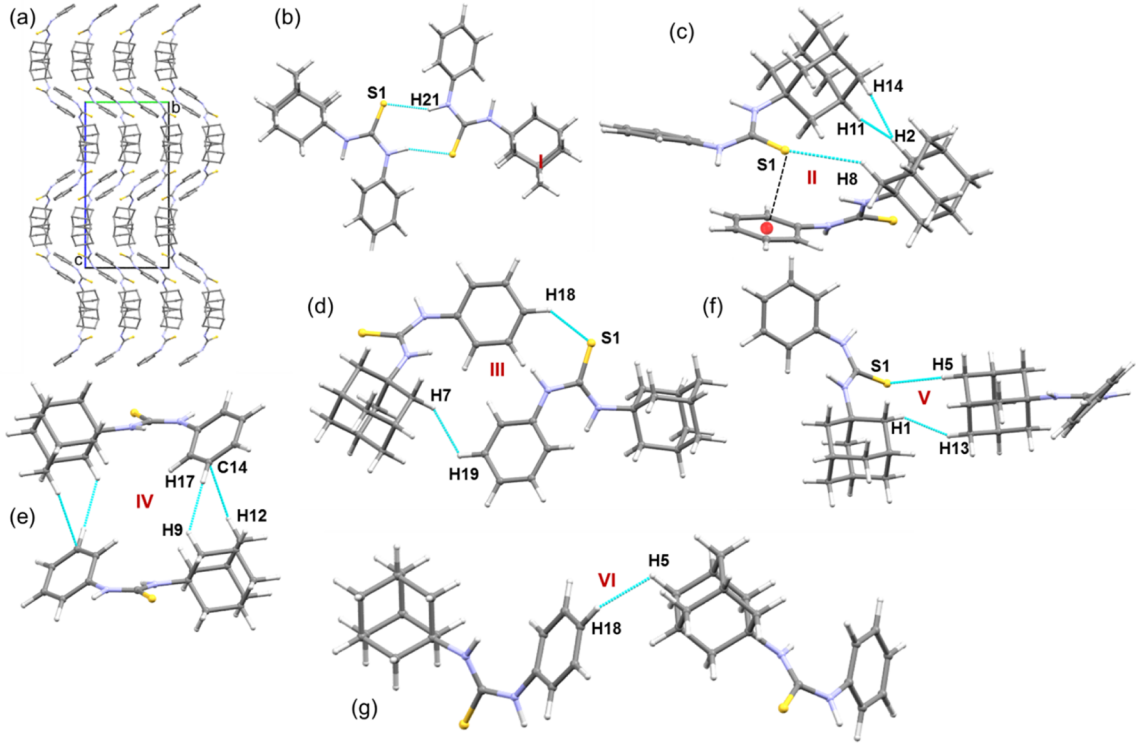

Figure 8. Crystal structure of compound **1** (a) viewed down the *a*-axis and H atoms have been omitted for clarity and different molecular dimers (b–g) held together by various non-covalent interactions.

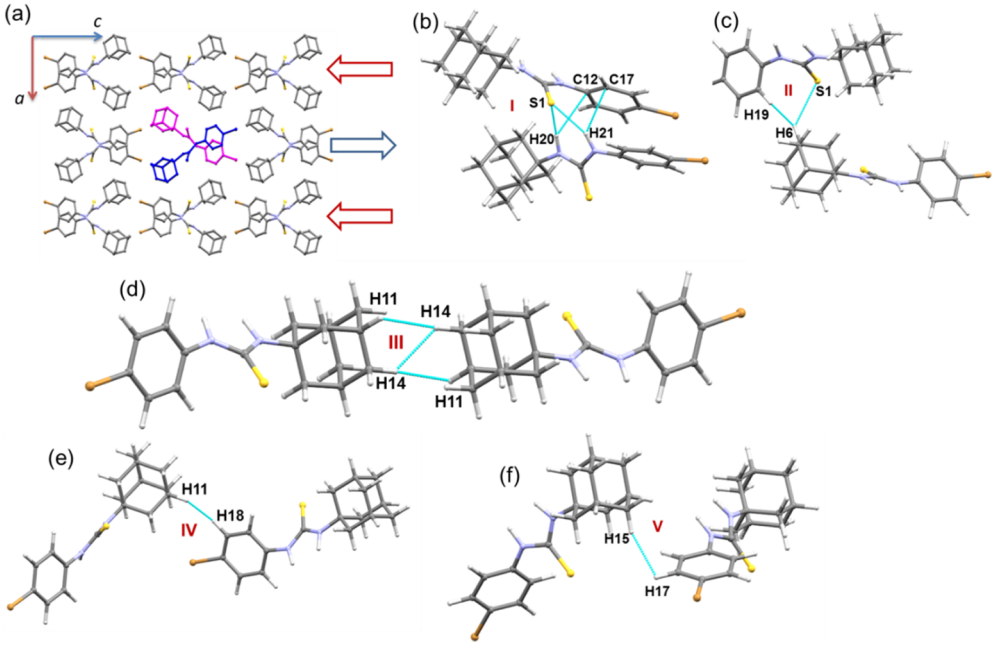

Figure 9. Crystal structure of **2** (a) viewed down the *b*-axis and H atoms have been omitted for clarity and different molecular dimers (b–f) held together by various non-covalent interactions in **2**.

covalency with an intermediate bonding character between shared and closed-shell interactions.[60] The distribution of total electronic energy density $H(r)$ for these two strong hydrogen bonds is shown in Figure 13. The remaining intermolecular interactions including a few N–H···S, C–H···X (X = Cl, Br, and F), C–H···S, C–H···C(π), and N–H···C(π) interactions are of closed-shell type of interactions according to the conditions [$\nabla^2\rho(r) > 0$, $|-V(r)/G(r)| < 0$, and $H(r) > 0$]. We note that the electron density and the Laplacian of electron density values for N–H···S hydrogen bonds observed in the present work are comparable with those of values observed for the same type of hydrogen bonds reported from thiourea derivatives.[61,62]

It is important to note that there are seven C–H···X-type interactions observed in derivatives with halogen substituents. In each structure, only one C–H···Br/Cl/F type of

https://dx.doi.org/10.1021/acsomega.0c05793
ACS Omega 2021, 6, 4816–4830

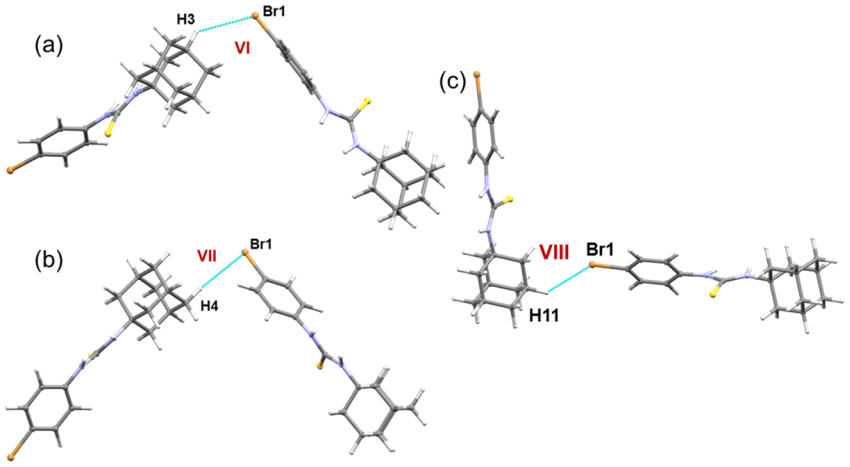

Figure 10. Intermolecular C−H···Br interactions formed in weak dimers (a−c) of structure **2**.

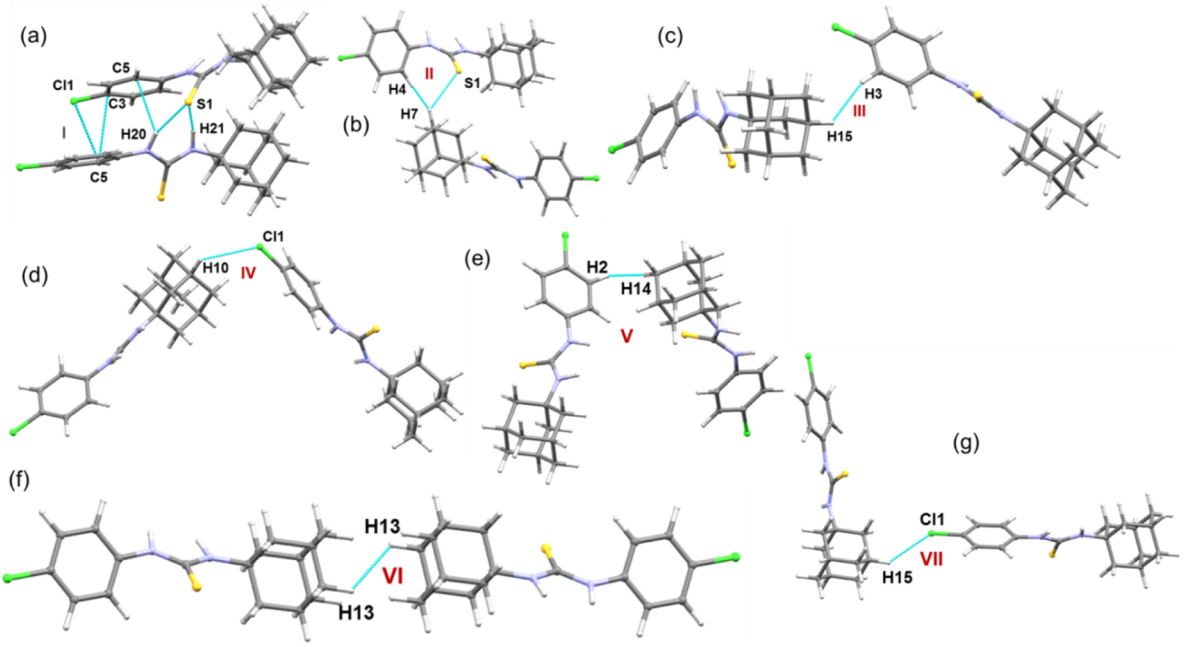

Figure 11. Different molecular dimers (a−g) held together by various non-covalent interactions in **3**.

interactions classified as hydrogen bonds and the remaining four such interactions are vdW in nature.

The dissociation energy (D_e) is used to measure the strength of these interactions. As expected, all the N−H···S hydrogen bonds are strong among other types of hydrogen bonds, and the D_e value ranges from 2.5 to 4.1 kcal mol^{-1}. Furthermore, the electron density (R^2 = 0.99) and the Laplacian of electron density (R^2 = 0.86) values for N−H···S hydrogen bonds show an exponential decay trend with the increasing value of the bond path (R_{ij}). Similarly, the dissociation energy also leads to exponential (R^2 = 0.99) and linear (R^2 = 0.99) regression with the bond path values. Apart from conventional interactions, short H···H contacts play essential roles in stabilizing the crystal structures, as evident from the dissociation energies for these contacts. These contacts operated in a non-electrostatic fashion and provide additional stability to various supramolecular topologies observed in these structures. We also described the importance of similar H···H short contacts observed in adamantane and other organic compounds previously, and these contacts were described as H−H bonding interactions.[51,52,63−65]

CONCLUSIONS

The reported crystal structures of four 1-(adamantan-1-yl)-3-arylthiourea derivatives with a phenyl and three 4-halophenyl substituents have been used in the present study to investigate the effect of halogens on the non-covalent interactions. These compounds crystallized in two different conformations, such as anti−syn and anti−anti for the thiourea moiety. The density functional theory (DFT) modeling suggests that the anti−syn conformer was relatively more stable than the corresponding anti−anti conformer. However, the unsubstituted and halogen-substituted derivatives exhibited local energy minima on their PESs for both anti−syn and anti−anti conformations. The Br and Cl derivatives showed 3D isostructurality in the solid state. The HS revealed the halogen effect, and these atoms reduce the contribution of inter-H···H contacts significantly. The reduced amount of contributions was compensated by inter-

https://dx.doi.org/10.1021/acsomega.0c05793
ACS Omega 2021, 6, 4816−4830

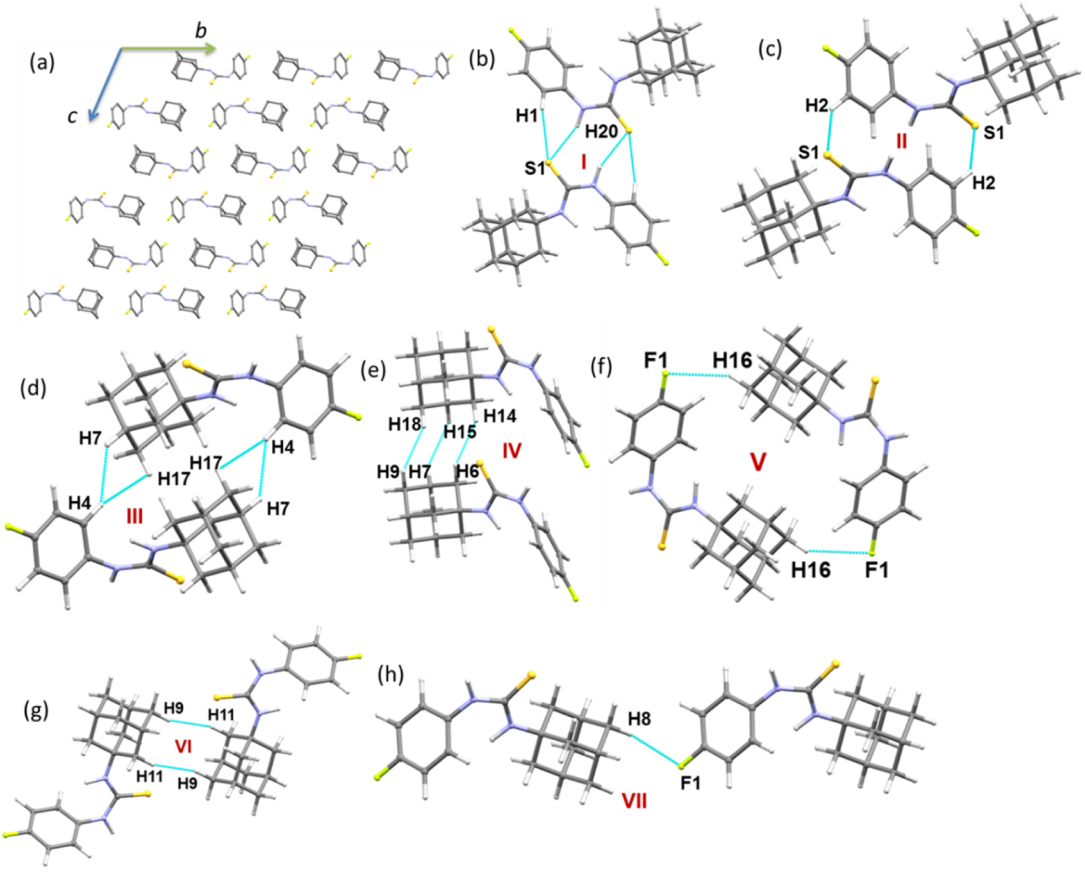

Figure 12. Crystal structure of **4** (a) viewed down the *a*-axis and H atoms have been omitted for clarity and different molecular dimers (b–h) held together by various non-covalent interactions in **4**.

Table 2. Lattice Energies (in kcal mol^{-1}) for Compounds 1–4 and Two Closely Related Crystals

compound code	E_{Coul}	E_{pol}	E_{disp}	E_{rep}	E_{tot}
1	−18.1	−10.4	−43.3	36.4	−35.4
2	−25.5	−16.1	−48.0	46.2	−43.4
3	−25.3	−16.8	−47.8	46.0	−43.9
4	−14.9	−7.9	−37.3	25.5	−34.5
RAPNOO	−18.5	−11.0	−41.7	32.2	−40.3
RAPNII	−17.4	−9.8	−36.7	30.1	−36.3

H···X contacts. The intermolecular interaction energies for different dimers were calculated using the PIXEL method. The results suggested that the strong dimer was stabilized by intermolecular N–H···S interactions in all four structures. It also indicated that an extensive number of H–H bondings as attractive interactions were observed in these structures either solely or cooperatively with other interactions. The lattice energy calculation showed that the fluoro derivative was found to be weakly packed in the crystalline state. The intermolecular N–H···S, C–H···S, and N–H···C(π) and some of the C–H···X interactions were classified as hydrogen bonds based on the KP-4 rule. Furthermore, the topological analysis suggested that the N–H···S hydrogen bond in the unsubstituted and chloro derivatives (one of the N–H···S hydrogen bonds) has an intermediate bonding character between shared and closed-shell interactions. The topological analysis further suggested that the H–H bonding interactions also played vital roles in stabilizing the dimeric topology observed in these structures. The MESP surface for these molecules revealed σ-holes at S and halogen atoms. The Lewis acids can interact with lone pairs of S and halogens, which is in good agreement with dimeric motifs formed by these atoms.

MATERIALS AND METHODS

Synthesis. The investigated 1-(adamantan-1-yl)-3-arylthiourea derivatives **1**–**4** were synthesized in almost quantitative yields by condensation of adamantan-1-yl isothiocyanate **A**[66] with the appropriate primary aromatic amine **B** *via* stirring in dichloromethane at room temperature (Scheme 1). The synthesis of compounds **1**, **2**, **3**, and **4** was previously reported *via* the reaction of adamantan-1-ylamine with the corresponding aryl isothiocyanate in ethanol in 76, 88, 85, and 92% yields, respectively.[30−33]

The appropriate primary aromatic amine **B** (0.01 mol) was added to a solution adamantan-1-yl isothiocyanate **A** (1.9 g, 0.01 mol) in dichloromethane (8 mL), and the mixture was stirred at room temperature for 24 h. The solvent was then distilled off *in vacuo*, and the obtained crude product was crystallized from ethanol.

1-(Adamantan-1-yl)-3-phenylthiourea (**1**): yield 2.75 g (96%); mp 171–173 °C; mol. formula (mol. wt): $C_{17}H_{22}N_2S$ (286.43).

1-(Adamantan-1-yl)-3-(4-bromophenyl)thiourea (**2**): yield 3.58 g (98%); mp 186–188 °C; mol. formula (mol. wt): $C_{17}H_{21}BrN_2S$ (365.33).

1-(Adamantan-1-yl)-3-(4-chlorophenyl)thiourea (**3**): yield 3.15 g (98%); mp 201–203 °C; mol. formula (mol. wt): $C_{17}H_{21}ClN_2S$ (320.88).

https://dx.doi.org/10.1021/acsomega.0c05793
ACS Omega 2021, 6, 4816−4830

Table 3. Topological Parameters for Intermolecular Interactions in Dimers of 1−4[a]

dimer	interaction	R_{ij}	$\rho(r)$	$\nabla^2\rho(r)$	$V(r)$	$G(r)$	$H(r)$	$\lvert -V(r)/G(r)\rvert$	D_e
				Compound **1**					
I	N2−H21···S1	2.456	0.128	1.072	−29.7	29.5	−0.3	1.01	3.6
IV	C9−H12···C14	2.896	0.038	0.411	−6.7	9.0	2.3	0.75	0.8
				Compound **2**					
I	N1−H20···S1	2.453	0.128	1.166	−31.5	31.6	0.1	1.00	3.8
	N2−H21···S1	2.452	0.129	1.150	−31.1	31.2	0.1	1.00	3.7
	N2−H21···C17(π)	3.208	0.048	0.537	−9.5	12.0	2.6	0.79	1.1
II	C5−H6···S1	2.981	0.053	0.544	−10.0	12.4	2.4	0.81	1.2
VIII	C8−H11···Br1	2.952	0.050	0.549	−9.8	12.4	2.6	0.79	1.2
				Compound **3**					
I	N1−H20···S1	2.418	0.138	1.194	−34.2	33.3	−0.8	1.02	4.1
	N1−H20···C5(π)	3.403	0.049	0.557	−9.8	12.5	2.7	0.78	1.2
	N2−H21···S1	2.471	0.124	1.141	−30.2	30.7	0.4	0.99	3.6
II	C10−H7···S1	2.945	0.056	0.571	−10.6	13.1	2.5	0.81	1.3
VII	C15−H15···Cl1	2.939	0.040	0.480	−7.7	10.4	2.7	0.74	0.9
				Compound **4**					
I	N1−H20···S1	2.589	0.100	0.960	−21.0	23.6	2.6	0.89	2.5
II	C3−H2···S1	2.916	0.055	0.536	−9.7	12.1	2.5	0.80	1.2
VII	C11−H8···F1	2.632	0.042	0.537	−10.1	12.3	2.3	0.81	1.2

[a] $\rho(r)$: electron density (e/Å^3); $\nabla^2\rho(r)$: Laplacian of electron density (e/Å^5); $V(r)$: potential energy density, $G(r)$: kinetic energy density; $H(r)$: total energy density; R_{ij}: bond path (Å), $D_e = -0.5 \times V(r)$ in kcal mol^{-1}, and the values of $V(r)$, $G(r)$, and $H(r)$ are given in kJ mol^{-1} bohr^{-3}.

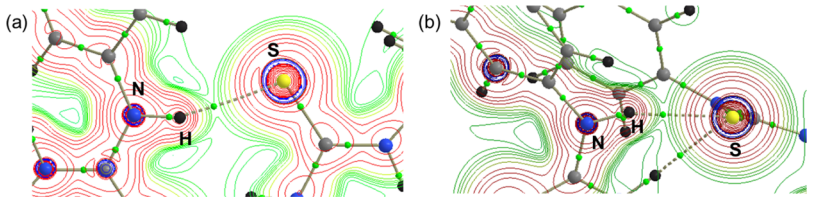

Figure 13. Distribution of $H(r)$ values showing the formation of strong N−H···S hydrogen bonds in structure **1** (a) and structure **3** (b). The uninterrupted regions at the bond critical points for these hydrogen bonds confirm the increasing covalency between H and S atoms.

1-(Adamantan-1-yl)-3-(4-fluorophenyl)thiourea (**4**): yield 2.89 g (95%); mp 169−171 °C; mol. formula (mol. wt): $C_{17}H_{21}FN_2S$ (304.43).

Theoretical Calculations. The single-point energy calculation and structural optimization in the gas phase were performed using the Gaussian 09 program.[67] For both calculations, the Minnesota functional M06-2X and the cc-pVTZ basis set were used.[68] Further, Grimme's empirical dispersion correction (D3) was incorporated in these calculations.[69] The frequency analysis at the same level of theory was then performed to confirm that the optimized structure corresponded to a stationary point with no negative frequencies. To identify the rotational barrier for the anti−anti and anti−syn conformers of the thiourea unit (H−N−C═S), we performed a relaxed PES scan around the N−C bonds of the thiourea fragment from −180 to +180 with an increment of 5° at the B3LYP/6-31G(d) level of approximation. The MESP surface was calculated for structures on the 0.001 au electron density contour with the WFA-SAS program.[70]

The crystal lattice energies and intermolecular interaction energies for dimers in these crystal structures were calculated using the PIXEL program.[71−74] For these calculations, the electron density of the monomers of **1**−**4** was obtained at the MP2/6-31G** level of theory using the Gaussian 09 program. According to the PIXEL energy formalism, the net intermolecular interaction energy for dimers and the total lattice energy for the crystal can be decomposed into Coulombic, polarization, dispersion, and repulsion energy components. The HS analysis was performed using the program CrystalExplorer-17.5.[75] For both the PIXEL and HS analyses, the structures with the normalized H atom involved distances moved to their typical neutron diffraction values (C−H = 1.083 Å and N−H = 1.009 Å).

The complexation energies for dimers were also calculated using the M06-2X-D3/cc-pVTZ level of theory, and these energies were further corrected from the basis set superposition error by the counterpoise method described by Boys and Bernardi.[76] The energetically significant dimers identified from the PIXEL energy analysis were further subjected to the topological analysis using Bader's QTAIM with the aid of the AIMALL software.[77] Using the calculated topological properties, the first four criteria of Koch and Popelier[59] were employed to characterize the non-covalent interactions found in these structures. More details of these calculations are described in our earlier work.[51,65]

■ ASSOCIATED CONTENT

Supporting Information

The Supporting Information is available free of charge at https://pubs.acs.org/doi/10.1021/acsomega.0c05793.

Selected torsion angles, topological parameters for intra- and intermolecular interactions, molecular graphs for different dimers, and crystal packing diagram (PDF)

https://dx.doi.org/10.1021/acsomega.0c05793
ACS Omega 2021, 6, 4816−4830

AUTHOR INFORMATION

Corresponding Author

Subbiah Thamotharan − *Biomolecular Crystallography Laboratory, Department of Bioinformatics, School of Chemical and Biotechnology, SASTRA Deemed University, Thanjavur 613 401, India;* orcid.org/0000-0003-2758-6649; Email: thamu@scbt.sastra.edu

Authors

Lamya H. Al-Wahaibi − *Department of Chemistry, College of Sciences, Princess Nourah Bint Abdulrahman University, Riyadh 11671, Saudi Arabia*

Divya Sri Grandhi − *Biomolecular Crystallography Laboratory, Department of Bioinformatics, School of Chemical and Biotechnology, SASTRA Deemed University, Thanjavur 613 401, India*

Samar S. Tawfik − *Department of Pharmaceutical Organic Chemistry, Faculty of Pharmacy, Mansoura University, Mansoura 35516, Egypt*

Nora H. Al-Shaalan − *Department of Chemistry, College of Sciences, Princess Nourah Bint Abdulrahman University, Riyadh 11671, Saudi Arabia*

Mohammed A. Elmorsy − *Department of Pharmaceutical Organic Chemistry, Faculty of Pharmacy, Mansoura University, Mansoura 35516, Egypt*

Ali A. El-Emam − *Department of Medicinal Chemistry, Faculty of Pharmacy, Mansoura University, Mansoura 35516, Egypt*

M. Judith Percino − *Unidad de Polímeros y Electrónica Orgánica, Instituto de Ciencias, Benemérita Universidad Autónoma de Puebla, Puebla CP 72960, Mexico;* orcid.org/0000-0003-1610-7155

Complete contact information is available at: https://pubs.acs.org/10.1021/acsomega.0c05793

Notes

The authors declare no competing financial interest.

ACKNOWLEDGMENTS

This research was funded by the Deanship of Scientific Research at Princess Nourah bint Abdulrahman University through the Research Groups Program (grant no. RGP-1442-0010-4). S.T. and M.J.P. would like to thank Laboratorio Nacional de Supercomputo del Sureste (LNS-BUAP) for computational resources.

REFERENCES

(1) Davies, W. L.; Grunert, R. R.; Haff, R. F.; McGahen, J. W.; Neumayer, E. M.; Paulshock, M.; Watts, J. C.; Wood, T. R.; Hermann, E. C.; Hoffmann, C. E. Antiviral activity of 1-adamantamine. *Science* **1964**, *144*, 862−863.

(2) Wendel, H. A.; Snyder, M. T.; Pell, S. Trial of amantadine in epidemic influenza. *Clin. Pharmacol. Ther.* **1966**, *7*, 38−43.

(3) Hayden, F. G.; Gwaltney, J. M.; Van de Castle, R. L.; Adams, K. F.; Giordani, B. Comparative toxicity of amantadine hydrochloride and rimantadine hydrochloride in healthy adults. *Antimicrob. Agents Chemother.* **1981**, *19*, 226−233.

(4) Rosenthal, K. S.; Sokol, M. S.; Ingram, R. L.; Subramanian, R.; Fort, R. C. Tromantadine: Inhibitor of early and late events in herpes simplex virus replication. *Antimicrob. Agents Chemother.* **1982**, *22*, 1031−1036.

(5) Balzarini, J.; Orzeszko-Krzesińska, B.; Maurin, J. K.; Orzeszko, A. Synthesis and anti-HIV studies of 2- and 3-adamantyl-substituted thiazolidin-4-ones. *Eur. J. Med. Chem.* **2009**, *44*, 303−311.

(6) Li, M.; Wang, H.; Hill, D. L.; Stinson, S.; Veley, K.; Grossi, I.; Peggins, J.; Covey, J. M.; Zhang, R. Preclinical pharmacology of the novel antitumor agent adaphostin, a tyrphostin analog that inhibits bcr/abl. *Canc. Chemother. Pharmacol.* **2006**, *57*, 607−614.

(7) Han, T.; Goralski, M.; Capota, E.; Padrick, S. B.; Kim, J.; Xie, Y.; Nijhawan, D. The antitumor toxin CD437 is a direct inhibitor of DNA polymerase α. *Nat. Chem. Biol.* **2016**, *12*, 511−515.

(8) Lorenzo, P.; Alvarez, R.; Ortiz, M. A.; Alvarez, S.; Piedrafita, F. J.; de Lera, A. R. Inhibition of IkappaB kinase-beta and anticancer activities of novel chalcone adamantyl arotinoids. *J. Med. Chem.* **2008**, *51*, 5431−5440.

(9) Min, J.; Guillen, V. S.; Sharma, A.; Zhao, Y.; Ziegler, Y.; Gong, P.; Mayne, C. G.; Srinivasan, S.; Kim, S. H.; Carlson, K. E.; Nettles, K. W.; Katzenellenbogen, B. S.; Katzenellenbogen, J. A. Adamantyl antiestrogens with novel Side chains reveal a spectrum of activities in suppressing estrogen receptor mediated activities in breast cancer cells. *J. Med. Chem.* **2017**, *60*, 6321−6336.

(10) Dai, L.; Smith, C. D.; Foroozesh, M.; Miele, L.; Qin, Z. The sphingosine kinase 2 inhibitor ABC294640 displays anti-non-small cell lung cancer activities in vitro and in vivo. *Int. J. Cancer* **2018**, *142*, 2153−2162.

(11) Protopopova, M.; Hanrahan, C.; Nikonenko, B.; Samala, R.; Chen, P.; Gearhart, J.; Einck, L.; Nacy, C. A. Identification of a new antitubercular drug candidate, SQ109, from a combinatorial library of 1,2-ethylenediamines. *J. Antimicrob. Chemother.* **2005**, *56*, 968−974.

(12) Bogatcheva, E.; Hanrahan, C.; Chen, P.; Gearhart, J.; Sacksteder, K.; Einck, L.; Nacy, C.; Protopopova, M. Discovery of dipiperidines as new antitubercular agents. *Bioorg. Med. Chem. Lett.* **2010**, *20*, 201−205.

(13) Omar, K.; Geronikaki, A.; Zoumpoulakis, P.; Camoutsis, C.; Soković, M.; Ćirić, A.; Glamočlija, J. Novel 4-thiazolidinone derivatives as potential antifungal and antibacterial drugs. *Bioorg. Med. Chem.* **2010**, *18*, 426−432.

(14) Hofer, S.; Brun, R.; Maerki, S.; Matile, H.; Scheurer, C.; Wittlin, S. In vitro assessment of the pharmacodynamic properties of DB75, piperaquine, OZ277 and OZ401 in cultures of Plasmodium falciparum. *J. Antimicrob. Chemother.* **2008**, *62*, 1061−1064.

(15) Charman, S. A.; Arbe-Barnes, S.; Bathurst, I. C.; Brun, R.; Campbell, M.; Charman, W. N.; Chiu, F. C. K.; Chollet, J.; Craft, J. C.; Creek, D. J.; Dong, Y.; Matile, H.; Maurer, M.; Morizzi, J.; Nguyen, T.; Papastogiannidis, P.; Scheurer, C.; Shackleford, D. M.; Sriraghavan, K.; Stingelin, L.; Tang, Y.; Urwyler, H.; Wang, X.; White, K. L.; Wittlin, S.; Zhou, L.; Vennerstrom, J. L. Synthetic ozonide drug candidate OZ439 offers new hope for a single-dose cure of uncomplicated malaria. *Proc. Natl. Acad. Sci. U.S.A.* **2011**, *108*, 4400−4405.

(16) Papanastasiou, I.; Tsotinis, A.; Kolocouris, N.; Prathalingam, S. R.; Kelly, J. M. Design, synthesis, and trypanocidal activity of new aminoadamantane derivatives. *J. Med. Chem.* **2008**, *51*, 1496−1500.

(17) Papanastasiou, I.; Tsotinis, A.; Zoidis, G.; Kolocouris, N.; Prathalingam, S. R.; Kelly, J. M. Design and synthesis of Trypanosoma brucei active 1-alkyloxy and 1-benzyloxyadamantano 2-guanylhydrazones. *ChemMedChem* **2009**, *4*, 1059−1062.

(18) Hu, H.; Lin, C.; Ao, M.; Ji, Y.; Tang, B.; Zhou, X.; Fang, M.; Zeng, J.; Wu, Z. Synthesis and biological evaluation of 1-(2-(adamantane- 1-yl)-1H-indol-5-yl)-3-substituted urea/thiourea derivatives as anticancer agents. *RSC Adv.* **2017**, *7*, 51640−51651.

(19) Al-Mutairi, A. A.; Al-Alshaikh, M. A.; Al-Omary, F. A. M.; Hassan, H. M.; El-Mahdy, A. M.; El-Emam, A. A. Synthesis, antimicrobial, and anti-proliferative activities of novel 4-(adamantan-1-yl)-1-arylidene-3-thiosemicarbazides, 4-arylmethyl N'-(adamantan-1-yl)piperidine-1-carbothioimidates, and related derivatives. *Molecules* **2019**, *24*, 4308.

(20) Al-Omary, F. A. M.; Chowdary Gude, N.; Al-Rasheed, L. S.; Alkahtani, H. N.; Hassan, H. M.; Al-Abdullah, E. S.; El-Emam, A. A.; Percino, M. J.; Thamotharan, S. X-ray and theoretical investigation of (Z)-3-(adamantan-1-yl)-1-(phenyl or 3-chlorophenyl)-S-(4-bromobenzyl)isothioureas: an exploration involving weak non-

covalent interactions, chemotherapeutic activities and QM/MM binding energy. *J. Biomol. Struct. Dyn.* **2020**, 1.
(21) D'Cruz, O.; Uckun, F. Novel broad-spectrum thiourea non-nucleoside inhibitors for the prevention of mucosal HIV transmission. *Curr. HIV Res.* **2006**, *4*, 329−345.
(22) Ahgren, C.; Backro, K.; Bell, F. W.; Cantrell, A. S.; Clemens, M.; Colacino, J. M.; Deeter, J. B.; Engelhardt, J. A.; Hogberg, M.; Jaskunas, S. R.; Johansson, N. G.; Jordan, C. L.; Kasher, J. S.; Kinnick, M. D.; Lind, P.; Lopez, C.; Morin, J. M., Jr.; Muesing, M. A.; Noreen, R.; Oberg, B.; Paget, C. J.; Palkowitz, J. A.; Parrish, C. A.; Pranc, P.; Rippy, M. K.; Rydergard, C.; Sahlberg, C.; Swanson, S.; Ternansky, R. J.; Unge, T.; Vasileff, R. T.; Vrang, L.; West, S. J.; Zhang, H.; Zhou, X.-X. The PETT series, a new class of potent nonnucleoside inhibitors of human immunodeficiency virus type 1 reverse transcriptase. *Antimicrob. Agents Chemother.* **1995**, *39*, 1329−1335.
(23) Kang, I.-J.; Wang, L.-W.; Hsu, S.-J.; Lee, C.-C.; Lee, Y.-C.; Wu, Y.-S.; Yueh, A.; Wang, J.-C.; Hsu, T.-A.; Chao, Y.-S.; Chern, J.-H. Design and efficient synthesis of novel arylthiourea derivatives as potent hepatitis C virus inhibitors. *Bioorg. Med. Chem. Lett.* **2009**, *19*, 6063−6068.
(24) Joshi, S. D.; Dixit, S. R.; Kirankumar, M. N.; Aminabhavi, T. M.; Raju, K. V. S. N.; Narayan, R.; Lherbet, C.; Yang, K. S. Synthesis, antimycobacterial screening and ligand-based molecular docking studies on novel pyrrole derivatives bearing pyrazoline, isoxazole and phenyl thiourea moieties. *Eur. J. Med. Chem.* **2016**, *107*, 133−152.
(25) Verlinden, B. K.; Niemand, J.; Snyman, J.; Sharma, S. K.; Beattie, R. J.; Woster, P. M.; Birkholtz, L.-M. Discovery of novel alkylated (bis)urea and (bis)thiourea polyamine analogues with potent antimalarial activities. *J. Med. Chem.* **2011**, *54*, 6624−6633.
(26) Zhou, H.; Wu, S.; Zhai, S.; Liu, A.; Sun, Y.; Li, R.; Zhang, Y.; Ekins, S.; Swaan, P. W.; Fang, B.; Zhang, B.; Yan, B. Design, synthesis, cytoselective toxicity, structure-activity relationships, and pharmacophore of thiazolidinone derivatives targeting drug-resistant lung cancer cells. *J. Med. Chem.* **2008**, *51*, 1242−1251.
(27) Hassan, H. Y.; El-Koussi, N. A.; Farghaly, Z. S. Synthesis and antimicrobial activity of pyridines bearing thiazoline and thiazolidinone moieties. *Chem. Pharm. Bull.* **1998**, *46*, 863−866.
(28) Al-Wahaibi, L.; Hassan, H.; Abo-Kamar, A.; Ghabbour, H.; El-Emam, A. Adamantane-isothiourea hybrid derivatives: synthesis, characterization, in vitro antimicrobial, and in vivo hypoglycemic activities. *Molecules* **2017**, *22*, 710.
(29) Al-Omary, F. A. M.; Al-Rasheed, L. S.; Ghabbour, H. A.; El-Emam, A. A. Crystal structure of 1-(adamantan-1-yl)-3-(3-chlorophenyl)thiourea, $C_{17}H_{21}ClN_2S$. *Z. Kristallogr.—New Cryst. Struct.* **2017**, *232*, 33−35.
(30) Al-Wahaibi, L. H.; Ghabbour, H. A.; Mostafa, G. A. E.; Almutairi, M. S.; El-Emam, A. A. Crystal structure of 1-(adamantan-1-yl)-3- phenylthiourea, $C_{17}H_{22}N_2S$. *Z. Kristallogr.—New Cryst. Struct.* **2016**, *231*, 593−595.
(31) Demirtaş, G.; Dege, N.; Al-Shehri, M. M.; El-Emam, A. A.; El-Brollosy, N. R.; Büyükgüngör, O. 1-(Adamantan-1-yl)-3-(4-fluorophenyl)-thiourea. *Acta Crystallogr., Sect. E: Struct. Rep. Online* **2012**, *68*, o1523.
(32) Al-Omary, F. A. M.; Ghabbour, H. A.; AlRabiah, H.; Al-Abdullah, E. S.; El-Emam, A. A. Crystal structure of 1-(adamantan-1-yl)-3-(4-chlorophenyl)thiourea, $C_{17}H_{21}ClN_2S$. *Z. Kristallogr.—New Cryst. Struct.* **2016**, *231*, 707−709.
(33) Al-Omary, F. A. M.; Al-Rasheed, L. S.; Ghabbour, H. A.; El-Emam, A. A. Crystal structure of 1-(adamantan-1-yl)-3-(4-bromophenyl)thiourea, $C_{17}H_{21}BrN_2S$. *Z. Kristallogr.—New Cryst. Struct.* **2016**, *231*, 1033−1035.
(34) Li, J.; Bourne, S. A.; de Villiers, M. M.; Caira, M. R.; Caira, M. R. Polymorphism of the antitubercular isoxyl. *Cryst. Growth Des.* **2011**, *11*, 4950−4957.
(35) Wishart, D. S.; Feunang, Y. D.; Guo, A. C.; Lo, E. J.; Marcu, A.; Grant, J. R.; Sajed, T.; Johnson, D.; Li, C.; Sayeeda, Z.; Assempour, N.; Iynkkaran, I.; Liu, Y.; Maciejewski, A.; Gale, N.; Wilson, A.; Chin, L.; Cummings, R.; Le, D.; Pon, A.; Knox, C.; Wilson, M. DrugBank 5.0: a major update to the DrugBank database for 2018. *Nucleic Acids Res.* **2017**, *46*, D1074−D1082.
(36) Charpentier, T. H.; Wilder, P. T.; Liriano, M. A.; Varney, K. M.; Zhong, S.; Coop, A.; Pozharski, E.; MacKerell, A. D., Jr.; Toth, E. A.; Weber, D. J. Small molecules bound to unique sites in the target protein binding cleft of calcium-bound S100B as characterized by nuclear magnetic resonance and X-ray crystallography. *Biochemistry* **2009**, *48*, 6202−6212.
(37) Ren, J.; Diprose, J.; Warren, J.; Esnouf, R. M.; Bird, L. E.; Ikemizu, S.; Slater, M.; Milton, J.; Balzarini, J.; Stuart, D. I.; Stammers, D. K. Phenylethylthiazolylthiourea (PETT) non-nucleoside inhibitors of HIV-1 and HIV-2 reverse transcriptases. Structural and biochemical analyses. *J. Biol. Chem.* **2000**, *275*, 5633−5639.
(38) Eccles, K. S.; Morrison, R. E.; Maguire, A. R.; Lawrence, S. E. Crystal landscape of primary aromatici thioamides. *Cryst. Growth Des.* **2014**, *14*, 2753−2762.
(39) Eccles, K. S.; Morrison, R. E.; Sinha, A. S.; Maguire, A. R.; Lawrence, S. E. Investigating C=S···I halogen bonding for cocrystallization with primary thioamides. *Cryst. Growth Des.* **2015**, *15*, 3442−3451.
(40) Saeed, A.; Bolte, M.; Erben, M. F.; Pérez, H. Intermolecular interactions in crystalline 1-(adamantane-1-carbonyl)-3-substituted thioureas with Hirshfeld surface analysis. *CrystEngComm* **2015**, *17*, 7551−7563.
(41) Saeed, A.; Ashraf, Z.; Erben, M. F.; Simpson, J. Vibrational spectra and molecular structure of isomeric 1-(adamantan-1-ylcarbonyl)-3-(dichlorophenyl)thioureas. *J. Mol. Struct.* **2017**, *1129*, 283−291.
(42) Saeed, A.; Flörke, U.; Erben, M. F. The role of substituents in the molecular and crystal structure of 1-(adamantane-1-carbonyl)-3-(mono)- and 3,3-(di) substituted thioureas. *J. Mol. Struct.* **2014**, *1065−1066*, 150−159.
(43) Saeed, A.; Erben, M. F.; Bolte, M. Synthesis, structural and vibrational properties of 1-(adamantane-1-carbonyl)-3-halophenyl thioureas. *Spectrochim. Acta Mol. Biomol. Spectrosc.* **2013**, *102*, 408−413.
(44) Abosadiya, H. M.; Anouar, E. H.; Yamin, B. M. Synthesis, X-ray, spectroscopic characterization (FT-IR, NMR, UV-Vis) and quantum chemical calculations of some substituted benzoylthiourea derivatives. *J. Mol. Struct.* **2019**, *1194*, 48−56.
(45) Pandey, S. K.; Pratap, S.; Marverti, G.; Kaur, M.; Jasinski, J. P. Synthesis, spectroscopic, crystal structure and in vitro cytotoxicity studies of N-thiophenoyl-N'-substituted phenyl thiocarbamide. *J. Mol. Struct.* **2019**, *1180*, 447−454.
(46) Groom, C. R.; Bruno, I. J.; Lightfoot, M. P.; Ward, S. C. The Cambridge structural database. *Acta Crystallogr.* **2016**, *72*, 171−179.
(47) Bader, R. F. W. A quantum theory of molecular structure and its applications. *Chem. Rev.* **1991**, *91*, 893−928.
(48) Bader, R. F. W. *Atoms in Molecules: A Quantum Theory*; Oxford University Press: USA, 1994.
(49) Saeed, A.; Khurshid, A.; Jasinski, J. P.; Pozzi, C. G.; Fantoni, A. C.; Erben, M. F. Competing intramolecular N−H···O=C hydrogen bonds and extended intermolecular network in 1-(4-chlorobenzoyl)-3-(2-methyl-4-oxopetan-2-yl)thiourea analyzed by experimental and theoretical methods. *Chem. Phys.* **2014**, *431−432*, 39−46.
(50) Nossa González, D. L.; Saeed, A.; Shabir, G.; Flörke, U.; Erben, M. F. Conformational and crystal structure of acyl thiourea compounds: the case of the simple (2,2-dimethyl-propionyl)thiourea derivative. *J. Mol. Struct.* **2020**, *1215*, 128227.
(51) El-Emam, A. A.; Saveeth Kumar, E.; Janani, K.; Al-Wahaibi, L. H.; Blacque, O.; El-Awady, M. I.; Al-Shaalan, N. H.; Percino, M. J.; Thamotharan, S. Quantitative assessment of the nature of non-covalent interactions in N-substituted-5-(adamantan-1-yl)-1,3,4-thiadiazole-2-amines: insights from crystallographic and QTAIM analysis. *RSC Adv.* **2020**, *10*, 9840−9853.
(52) Al-Wahaibi, L. H.; Sujay, S.; Muthu, G. G.; El-Emam, A. A.; Venkataramanan, N. S.; Al-Omary, F. A. M.; Ghabbour, H. A.; Percino, J.; Thamotharan, S. Theoretical investigations of two

https://dx.doi.org/10.1021/acsomega.0c05793
ACS Omega 2021, 6, 4816−4830

adamantane derivatives: A combined X-ray, DFT, QTAIM analysis and molecular docking. *J. Mol. Struct.* **2018**, *1159*, 233−245.
(53) El-Emam, A. A.; Al-Omary, F. A. M.; Al-Rasheed, L. S.; Ghabbour, H. A.; Al-Abdullah, E. S. Crystal structure of (Z)-3-(adamantan-1-yl)-1-(3-chlorophenyl)-S-benzylisothiourea, C24H27ClN2S. *Z. Kristallogr.—New Cryst. Struct.* **2017**, *232*, 453−456.
(54) Cremer, D.; Pople, J. A. General definition of ring puckering coordinates. *J. Am. Chem. Soc.* **1975**, *97*, 1354−1358.
(55) Matta, C. F.; Hernández-Trujillo, J.; Tang, T.-H.; Bader, R. F. W. Hydrogen-hydrogen bonding: A stabilizing interaction in molecules and crystals. *Chem.—Eur. J.* **2003**, *9*, 1940−1951.
(56) Matta, C. F. *Hydrogen Bonding-New Insights*; Springer, 2006.
(57) Cukrowski, I.; Matta, C. F. Hydrogen-hydrogen bonding: A stabilizing interaction in strained chelating rings of metal complexes in aqueous phase. *Chem. Phys. Lett.* **2010**, *499*, 66−69.
(58) Thamotharan, S.; Kothandapani, J.; Selva Ganesan, S.; Venkataramanan, N. S.; Madan Kumar, S.; Byrappa, K.; Percino, J.; Robles, F. Quantitative analysis of intermolecular interactions in 2,2'-((4-bromophenyl)methylene)bis (3-hydroxy-5,5- dimethylcyclohex-2-en-1-one): insights from crystal structure, PIXEL, Hirshfeld surfaces and QTAIM analysis. *J. Chem. Sci.* **2018**, *130*, 20.
(59) Koch, U.; Popelier, P. L. A. Characterization of C-H-O hydrogen bonds on the of the charge density. *J. Phys. Chem. B* **1995**, *99*, 9747−9754.
(60) Gatti, C. Chemical bonding in crystals: new directions. *Z. Kristallogr.—Cryst. Mater.* **2005**, *220*, 399−457.
(61) Saeed, A.; Khurshid, A.; Bolte, M.; Fantoni, A. C.; Erben, M. F. Intra- and intermolecular hydrogen bonding and conformation in 1-acyl thioureas: an experimental and theoretical approachon 1-(2-chlorobenzoyl)thiourea. *Spectrochim. Acta Mol. Biomol. Spectrosc.* **2015**, *143*, 59−66.
(62) Cairo, R. R.; Stevens, A. M. P.; de Oliveira, T. D.; Batista, A. A.; Castellano, E. E.; Duque, J.; Soria, D. B.; Fantoni, A. C.; Corrêa, R. S.; Erben, M. F. Understanding the conformational changes and molecular structure of guroyl thioureas upon substitution. *Spectrochim. Acta Mol. Biomol. Spectrosc.* **2017**, *176*, 8−17.
(63) Al-Ghulikah, H. A.; Gopalan, A.; Sathiya Vahisan, L. P.; Khalaf, M. A.; Ghabbour, H. A.; El-Emam, A. A.; Percino, M. J.; Thamotharan, S. Insights into the weak Csp3−H···H−Csp3 mediated supramolecular architecture in ethyl 2-(5-bromopentanamido)-4,5,6,7-tetrahydrobenzo[b]thiophene-3- carboxylate, a probable selective COX-2 lead molecule: An integrated crystallographic and theoretical approach. *J. Mol. Struct.* **2020**, *1199*, 127019.
(64) Udayakumar, M.; Cerón, M.; Ceballos, P.; Percino, M. J.; Thamotharan, S. Correlation between structural and optical properties of π-conjugated acrylonitrile derivatives: Insights from X-ray, energy frameworks, TD-DFT and charge density analysis. *J. Mol. Struct.* **2020**, *1213*, 128174.
(65) Udayakumar, M.; Jagatheeswaran, K.; Ganesan, S. S.; Venkataramanan, N. S.; Madan Kumar, S.; Byrappa, K.; Thamotharan, S. Investigation of 9-(2-hydroxy-4,4-dimethyl-6-oxocyclohex-1-en-1-yl)-3,3-dimethyl-2,3,4,9-tetrahydro-1H-xanthen-1-one: Crystal structure, AIM and NBO analysis. *J. Mol. Struct.* **2017**, *1133*, 510−518.
(66) Douglass, I. B.; Dains, F. B. Some derivatives of benzoyl and furoyl isothiocyanates and their use in synthesizing heterocyclic compounds. *J. Am. Chem. Soc.* **1934**, *56*, 719−721.
(67) Frisch, M. J.; Trucks, G. W.; Schlegel, H. B.; Scuseria, G. E.; Robb, M. A.; Cheeseman, J. R.; Scalmani, G.; Barone, V.; Mennucci, B.; Petersson, G. A.; Nakatsuji, H.; Caricato, M.; Li, X.; Hratchian, H. P.; Izmaylov, A. F.; Bloino, J.; Zheng, G.; Sonnenberg, J. L.; Hada, M.; Ehara, M.; Toyota, K.; Fukuda, R.; Hasegawa, J.; Ishida, M.; Nakajima, T.; Honda, Y.; Kitao, O.; Nakai, H.; Vreven, T.; Montgomery, J. A., Jr.; Peralta, J. E.; Ogliaro, F.; Bearpark, M. J.; Heyd, J.; Brothers, E. N.; Kudin, K. N.; Staroverov, V. N.; Kobayashi, R.; Normand, J.; Raghavachari, K.; Rendell, A. P.; Burant, J. C.; Iyengar, S. S.; Tomasi, J.; Cossi, M.; Rega, N.; Millam, N. J.; Klene, M.; Knox, J. E.; Cross, J. B.; Bakken, V.; Adamo, C.; Jaramillo, J.; Gomperts, R.; Stratmann, R. E.; Yazyev, O.; Austin, A. J.; Cammi, R.; Pomelli, C.; Ochterski, J. W.; Martin, R. L.; Morokuma, K.; Zakrzewski, V. G.; Voth, G. A.; Salvador, P.; Dannenberg, J. J.; Dapprich, S.; Daniels, A. D.; Farkas, Ö.; Foresman, J. B.; Ortiz, J. V.; Cioslowski, J.; Fox, D. J. *Gaussian 09*, Revision D.01; Gaussian, Inc.: Wallingford, CT, USA, 2013.
(68) Zhao, Y.; Truhlar, D. G. The M06 suite of density functionals for main group thermochemistry, thermochemical kinetics, noncovalent interactions, excited states, and transition elements: two new functionals and systematic testing of four M06-class functionals and 12 other functionals. *Theor. Chem. Acc.* **2008**, *120*, 215−241.
(69) Grimme, S.; Antony, J.; Ehrlich, S.; Krieg, H. A consistent and accurate ab initio parametrization of density functional dispersion correction (DFT-D) for the 94 elements H-Pu. *J. Chem. Phys.* **2010**, *132*, 154104.
(70) Bulat, F. A.; Toro-Labbé, A.; Brinck, T.; Murray, J. S.; Politzer, P. Quantitative analysis of molecular surfaces: areas, volumes, electrostatic potentials and average local ionization energies. *J. Mol. Model.* **2010**, *16*, 1679−1691.
(71) Gavezzotti, A. Calculation of intermolecular interaction energies by direct numerical integration over electron densities. I. Electrostatic and polarization energies in molecular crystals. *J. Phys. Chem. B* **2002**, *106*, 4145−4154.
(72) Gavezzotti, A. Calculation of intermolecular interaction energies by direct numerical integration over electron densities. 2. An improved polarization model and the evaluation of dispersion and repulsion energies. *J. Phys. Chem. B* **2003**, *107*, 2344−2353.
(73) Gavezzotti, A. Calculation of lattice energies of organic crystals: the PIXEL integration method in comparison with more traditional methods. *Z. für Kristallogr.—Cryst. Mater.* **2005**, *220*, 499−510.
(74) Gavezzotti, A. Efficient computer modeling of organic materials. The atom−atom, Coulomb−London-Pauli (AA-CLP) model for intermolecular electrostatic-polarization, dispersion and repulsion energies. *New J. Chem.* **2011**, *35*, 1360−1368.
(75) Turner, M. J.; McKinnon, J. J.; Wolff, S. K.; Grimwood, D. J.; Spackman, P. R.; Jayatilaka, D.; Spackman, M. A. *CrystalExplorer17*; University of Western Australia, 2017.
(76) Boys, S. F.; Bernardi, F. The calculation of small molecular interactions by the differences of separate total energies. Some procedures with reduced errors. *Mol. Phys.* **1970**, *19*, 553−566.
(77) Keith, T. A. T. K. *Gristmill, AIMAll*, (Version 19.10.12) Software; Overland Park KS, USA, 2019.

https://dx.doi.org/10.1021/acsomega.0c05793
ACS Omega 2021, 6, 4816−4830